Journal of Systems Engineering and Electronics
Vol. 33, No. 3, June 2022, pp.575 – 584

Multi-static InISAR imaging for ships under sparse aperture

JI Bingren, WANG Yong*, ZHAO Bin, and XU Rongqing
School of Electronics and Information Engineering, Harbin Institute of Technology, Harbin 150001, China

Abstract: This paper concentrates on super-resolution imaging of the ship target under the sparse aperture situation. Firstly, a multi-static configuration is utilized to solve the coherent processing interval (CPI) problem caused by the slow-speed motion of ship targets. Then, we realize signal restoration and image reconstruction with the alternating direction method of multipliers (ADMM). Furthermore, we adopt the interferometric technique to produce the three-dimensional (3D) images of ship targets, namely interferometric inverse synthetic aperture radar (InISAR) imaging. Experiments based on the simulated data are utilized to verify the validity of the proposed method.

Keywords: multi-static, sparse aperture, signal recovery, interferometric inverse synthetic aperture radar (InISAR), ship target, alternating direction method of multipliers (ADMM).

DOI: 10.23919/JSEE.2022.000055

1. Introduction

Inverse synthetic aperture radar (ISAR) is able to operate normally regardless of time limitation and weather conditions [1−5]. As we all know, ISAR imaging achieves high resolutions in the range direction by transmitting wideband signals and in the azimuth direction by processing the large Doppler frequency generated by the target's effective rotational motion. Usually, long coherent processing interval (CPI) is a good way to acquire enough Doppler frequency shift.

In recent years, phase array radar has been increasingly deployed to carry out multiple tasks with the help of time control mechanisms [6]. By continuously adjusting the directions of the radar beams, the system can track, recognize, and image different targets in a relatively short time. However, in order to monitor the status of different targets, long and continuous radar beam illumination for any single target cannot be achieved at all time, which will lead to the sparse aperture situation for the echoed data.

In addition, the complex motions of targets and deliberate interference can also lead to the missing of echoes and then result in the degeneration of imaging performance, and failure of sequential automatic target recognition (ATR). Thus, how to acquire super-resolution ISAR images under the sparse aperture situation has attracted a lot of attention recently [7].

To overcome the sparse aperture imaging challenge, the first problem we have to solve is motion compensation of the observed target under sparse aperture situation. Range alignment and phase adjustment are two processes in motion compensation, which aim to eliminate the misalignments and phase errors between pulses. These two steps can guarantee the focus of image and the retention of target features. Numerous range alignment methods have been presented in [8,9]. However, when facing sparse aperture conditions, approaches such as the scatterer point referencing algorithm lose efficacy, while the global minimum entropy-based method can produce acceptable performance. In addition, most phase-adjustment methods such as the phase gradient autofocus algorithm [10] and the weighted least-squares algorithm [11] become inapplicable due to the loss of coherence between different pulses under the sparse aperture condition. The eigenvector-based autofocus method [12,13], on the other hand, is still suitable in this case, and is used in this paper.

Then, we should solve the problem of data missing. The existing sparse aperture ISAR imaging techniques include linear prediction methods, modern spectrum estimation methods, and sparse signal recovery methods. The performance of the former two methods are easily affected by the signal to noise ratio (SNR) [14]. Among the third category, the compressive sensing (CS) method is exempt from the limitation of the Nyquist sampling theory [15−17]. The number of dominant scatterers in ISAR images is small compared to the whole image, which allows the echo signals in the image domain to be considered as compressible. The alternating direction method of multipliers (ADMM) is an emerging technique, which can solve the signal reconstruction problem by uti-

Manuscript received March 01, 2021.
*Corresponding author.
This work was supported by the National Natural Science Foundation of China (61871146).

lizing the proximal splitting strategy [18−20]. In this paper, we adopt the ADMM algorithm to restore the missing parts of the signal, which can produce excellent imaging performance.

In fact, the observed targets sometimes sail along the radar light of sight (RLOS) deliberately, leading to the loss of relative rotational motion between the target and the RLOS, which brings trouble to ISAR imaging [21]. In addition, for slow-velocity targets, for example, ship targets, imaging fails when they move within a small angle of LOS [22]. If we adopt a long CPI to solve this issue, the system will require large data storage and long processing time, which is not suitable for real time processing. Furthermore, ship target motion states could be complex in the rough sea condition with a long CPI. Thus, we make use of the multi-static configuration to solve aforementioned problems. With the separation of the transmitter and the receivers, the relative motion of the target to the receiver is accentuated compared with the mono-static situation. In addition, multi-static radar system can also increase the battle survival rate due to the separation of the transmitter and the receivers.

Normally, the target mapped onto the image projection plane (IPP) forms the ISAR image. The imaging results could be different when selecting different IPPs or imaging time. In addition, the complex motion of targets also brings trouble to target recognition [23−26]. To overcome these shortness, we adopt the interferometric ISAR (InISAR) method to produce the three-dimensional (3D) imaging results.

In this paper, we attempt to combine the multi-static configuration and InISAR techniques with the signal recovery method ADMM to deal with the ship 3D imaging problem under the sparse aperture situation.

The remaining sections are organized as follows: The signal model is established in Section 2. Section 3 introduces the ADMM signal recovery algorithm and illustrates the flow chart of multi-static InISAR imaging for the ship target with sparse aperture situation. In Section 4, experiments with the simulated model are provided to verify the validity of the proposed method. Finally, conclusions are drawn in Section 5.

2. Signal model

Fig. 1 shows the multi-static InISAR imaging system. Transmitter T, receiver B, and receiver A locate in the axis U, while the receiver C locates in the axis W. The axis V is perpendicular to the plane formed by axis U and axis W. We define receiver A as the origin O of the coordinate system. The baseline length is $|AB| = |AC| = L_r$ and the length between O and transmitter T is $|AT| = L_{tr}$. The target is situated in the reference system (O', X, Y, Z). The radar system (O, U, V, W) and the reference system (O', X, Y, Z) are parallel to each other. P is one of the scatterers on the ship and $|PA| = R_{PA}$, $|PB| = R_{PB}$, $|PC| = R_{PC}$, $|TP| = R_{TP}$. η, ξ, ζ denote the three axes of rotation. w_r, w_p, w_y are the roll, pitch, and yaw rotations. Besides, M is in the middle between receiver A and receiver B with $|PM| = R_{PM}$. The observed targets usually locate in the far field, therefore, $R_{PA} + R_{PB} \gg L_r$ and $R_{PA} + R_{PB} \approx 2R_{PM}$.

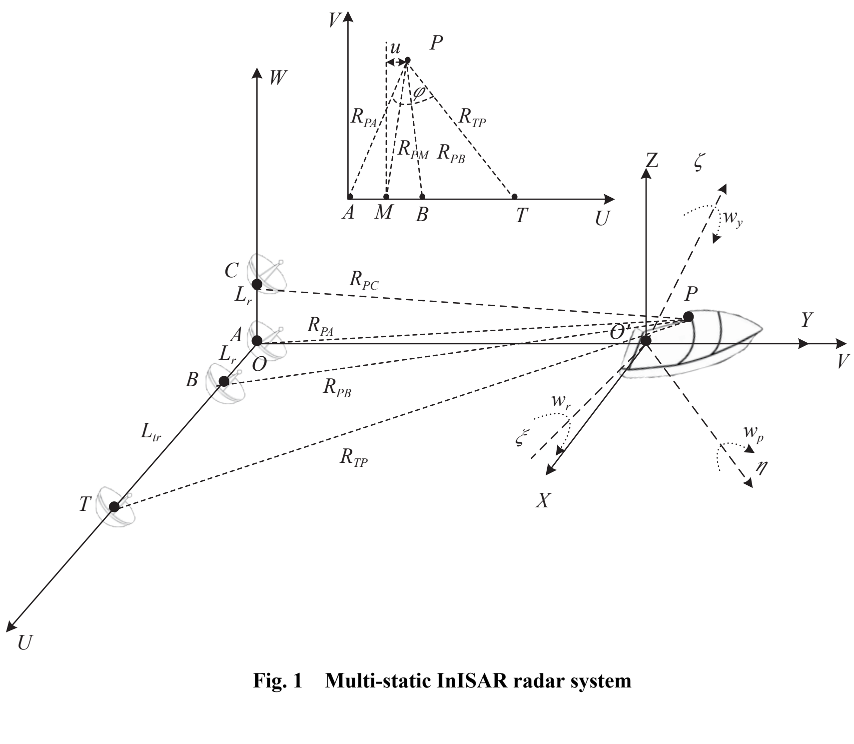

Fig. 1 Multi-static InISAR radar system

Consider that the signal transmitted from the transmitter is a linear frequency modulation (LFM) signal:

$$s_T(\hat{t}, t_m) = \mathrm{rect}\left(\frac{\hat{t}}{T_p}\right)\exp\left(\mathrm{j}2\pi\left(f_c t + \frac{1}{2}kt^2\right)\right) \tag{1}$$

where rect(t) is the rectangle function, T_P means the pulse width, and k stands for the chirp rate. $t_m = mT_r(m = 0, 1, 2, \cdots, M)$ denotes the slow time. $\hat{t}$ is the fast time, and $\hat{t} = t - t_m$. M represents the echoes' number. f_c is the initial frequency.

The returned signal from the ship target can be shown as

$$s_{q(\hat{t}, t_m)} = \sum_{p=1}^{P}\sigma_p \mathrm{rect}\left(\frac{\hat{t} - R_q(t_m)/\mathrm{c}}{T_\mathrm{p}}\right)\cdot \exp\left(\mathrm{j}2\pi\left(f_c\left(t - \frac{R_q(t_m)}{\mathrm{c}}\right) + \frac{1}{2}k\left(\hat{t} - \frac{R_q(t_m)}{\mathrm{c}}\right)^2\right)\right) \tag{2}$$

where q=A, B, C, $R_q(t_m) = R_{TP}(t_m) + R_{pq}(t_m)$, P is the number of all the target's scatters, c denotes the light velocity, and σ_p represents the reflectivity of scatter p.

Assume that $R_\mathrm{ref}(t_m)$ represents the reference distance and T_ref stands for the pulse width. The reference signal is expressed as

$$s_\mathrm{ref} = \mathrm{rect}\left(\frac{\hat{t} - R_\mathrm{ref}(t_m)/\mathrm{c}}{T_\mathrm{ref}}\right)\cdot \exp\left(\mathrm{j}2\pi\left(f_c\left(t - \frac{2R_\mathrm{ref}(t_m)}{\mathrm{c}}\right) + \frac{1}{2}k\left(\hat{t} - \frac{2R_\mathrm{ref}(t_m)}{\mathrm{c}}\right)^2\right)\right). \tag{3}$$

After the de-chirp process, the signal is expressed as

$$s_q(\hat{t}, t_m) = \sum_{p=1}^{P}\sigma_p \mathrm{rect}\left(\frac{\hat{t} - R_q(t_m)/\mathrm{c}}{T_p}\right)\cdot \exp\left(-\mathrm{j}\frac{4\pi}{\mathrm{c}}f_c\Delta R_q(t_m)\right)\cdot\exp\left(-\mathrm{j}\frac{4\pi}{\mathrm{c}^2}k\Delta R_q^2(t_m)\right)\cdot \exp\left(-\mathrm{j}\frac{4\pi}{\mathrm{c}}k\left(\hat{t} - \frac{2R_\mathrm{ref}(t_m)}{\mathrm{c}}\right)\Delta R_q(t_m)\right) \tag{4}$$

where

$$\Delta R_q(t_m) = (R_{TP}(t_m) + R_{pq}(t_m))/2 - R_\mathrm{ref}(t_m), \quad p = 1,2,\cdots,P;\ q = A,B,C. \tag{5}$$

Then, fast Fourier transform (FFT) is carried out with regard to $\hat{t}$,

$$s_q(\hat{f}, t_m) = \sum_{p=1}^{P}\sigma_p T_p \mathrm{sinc}\left(T_p\left(\hat{f} + 2\frac{k}{\mathrm{c}}(\Delta R_q(t_m))\right)\right)\cdot \exp\left(-\mathrm{j}\frac{4\pi f_c}{\mathrm{c}}\Delta R_q(t_m)\right)\cdot\exp\left(-\mathrm{j}\frac{4\pi\hat{f}}{\mathrm{c}}\Delta R_q(t_m)\right)\cdot \exp\left(-\mathrm{j}\frac{4\pi}{\mathrm{c}^2}k\Delta R_q^2(t_m)\right). \tag{6}$$

The second exponential term in (6) can lead to the migration through resolution cell and needs to be eliminated with the keystone transform, while the last term stands for the residual video phase, which may degrade the imaging quality and should be erased. After removing the last two exponential terms, (6) can be abbreviated as

$$s_q(\hat{f}, t_m) = \sum_{p=1}^{P}\sigma_p T_p \mathrm{sinc}\left(T_p\left(\hat{f} + 2\frac{k}{\mathrm{c}}(\Delta R_q(t_m))\right)\right)\cdot \exp\left(-\mathrm{j}\frac{4\pi f_c}{\mathrm{c}}\Delta R_q(t_m)\right). \tag{7}$$

To obtain the coordinates of the target's scatterers, interferometric processing is implemented with regard to the signal $s_A\left(\hat{f}, t_m\right)$ and signal $s_B(\hat{f}, t_m)$.

$$s_B(\hat{f}, t_m)\mathrm{conj}\left(s_A(\hat{f}, t_m)\right) = \sum_{p=1}^{P}\left|s_A(\hat{f}, t_m)\right|\left|s_B(\hat{f}, t_m)\right|\cdot \exp\left(\mathrm{j}\frac{2\pi f_\mathrm{c}}{\mathrm{c}}(R_{pA}(t_m) - R_{pB}(t_m))\right) = \sum_{p=1}^{P}\left|s_A(\hat{f}, t_m)\right|\left|s_B(\hat{f}, t_m)\right|\exp(\mathrm{j}\Delta\varphi_{AB}) \tag{8}$$

From mathematical deductions, we have $R_{pA} - R_{pB} = \dfrac{2uL_r}{R_{pA} + R_{pB}}$, and then the scatterer p's coordinate in the U axis is

$$u_p = u + \frac{L_r}{2} = \frac{\mathrm{c}R_{PM}\Delta\varphi_{AB}}{2\pi f_c L_r} + \frac{L_r}{2} \tag{9}$$

where u denotes the distance between the scatterer p and M along the U axis.

Similarly, by interferometricly processing the signals $s_A\left(\hat{f}, t_m\right)$ and $s_C\left(\hat{f}, t_m\right)$, the scatterer p's coordinate in the W axis can be acquired. The scatterer p's coordinate in the V axis is obtained through the range information. Next, we take the following transformation to convert the scatterer's radar system coordinates to the target coordinates, taking into consideration the target's rotational motion:

$$[\xi, \eta, \varsigma]^\mathrm{T} = [\mathrm{Rot}(\theta_r(t), \theta_p(t), \theta_y(t))\ \ \mathrm{Rot}(\theta_{r0}, \theta_{p0}, \theta_{y0})]^{-1}\cdot\ [U, V, W]^\mathrm{T} \tag{10}$$

where $[\xi,\eta,\varsigma]$ and $[U,V,W]$ denote the coordinates of the scatterers in the coordinate systems (O',ξ,η,ς) and (O,U,V,W) respectively. Rot represents the rotation matrix of the ship target. Moreover, $\theta_r(t),\theta_p(t),\theta_y(t)$ represent the instantaneous angles caused by the roll, pitch, yaw of the ship. $\theta_{r0},\theta_{p0},\theta_{y0}$ are the angles of rotation at time $t_m=0$.

In addition, as the result of the multi-static configuration, the coordinates derived above would be distorted and another coordinate transformation is needed to recover the true coordinates [22].

The sparse aperture situation usually contains two types: random and gap. Fig. 2 gives the schematic of the random case, where the blue squares indicate the valid data and the white ones denote the empty data.

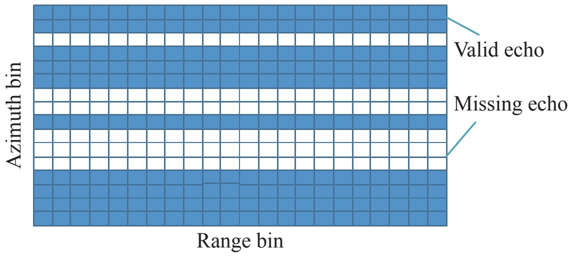

Fig. 2 Geometry of sparse aperture signal

3. Details of the ADMM method

In this section, we first give the details of the ADMM method. Then the angular motion compensation and the flow of the proposed method are described, respectively.

3.1 ADMM method for signal recovery

From (7), we can obtain the range compressed data in the nth range bin as

$$s_{qn}(t_m)=\sum_{p=1}^{P}\hat{\sigma}_p\exp\left(-\mathrm{j}\frac{4\pi f_c}{\mathrm{c}}\Delta R_q(t_m)\right),$$
$$n=1,2,\cdots,N;q=A,B,C \tag{11}$$

where N denotes the range bins' number.

Equation (11) can be further expressed as

$$\boldsymbol{s}_{qn}=\boldsymbol{D}\hat{\boldsymbol{\sigma}}+\boldsymbol{w} \tag{12}$$

where $\boldsymbol{s}_{qn}=[s_{qn}(1),s_{qn}(2),\cdots,s_{qn}(M)]^{\mathrm{T}}$, $\boldsymbol{D}=\left[\exp\left(-\mathrm{j}\frac{4\pi f_c}{\mathrm{c}}\cdot\Delta R_q(t_m)\right)\right]_{M\times P}$, $\hat{\boldsymbol{\sigma}}=[\sigma_1,\sigma_2,\cdots,\sigma_P]^{\mathrm{T}}$, $\boldsymbol{w}=[w(1),w(2),\cdots,w(M)]^{\mathrm{T}}$, and w denotes the additive Gaussian white noise.

Equation (12) can be described as an unconstrained optimization problem:

$$\hat{\boldsymbol{\sigma}}=\arg\min\left(\frac{1}{2}\left\|\boldsymbol{s}_{qn}-\boldsymbol{D}\hat{\boldsymbol{\sigma}}\right\|_2^2+\lambda\|\hat{\boldsymbol{\sigma}}\|_1\right) \tag{13}$$

where λ denotes the regularization coefficient.

We utilize the ADMM method to split (13) into sub-problems, which is an effective way in solving this kind of problem.

The augmented Largrangian function can be expressed as

$$L_\delta(\hat{\boldsymbol{\sigma}},\boldsymbol{\mu},\boldsymbol{\gamma})=\frac{1}{2}\left\|\boldsymbol{s}_{qn}-\boldsymbol{D}\hat{\boldsymbol{\sigma}}\right\|_2^2+\lambda\|\boldsymbol{\mu}\|_1+$$
$$\boldsymbol{\gamma}(\hat{\boldsymbol{\sigma}}-\boldsymbol{\mu})+\frac{\delta}{2}\|\hat{\boldsymbol{\sigma}}-\boldsymbol{\mu}\|_2^2$$
$$\text{s.t. } \hat{\boldsymbol{\sigma}}=\boldsymbol{\mu} \tag{14}$$

where δ is the penalty parameter, $\boldsymbol{\gamma}$ represents the Lagrangian multipliers, and $\boldsymbol{\mu}$ stands for the auxiliary variable.

The ADMM method decouples (14) into several sub-problems, and updates the variables alternately. The updating processes are

$$\hat{\boldsymbol{\sigma}}^{i+1}=\arg\min_{\hat{\boldsymbol{\sigma}}}L_\delta(\hat{\boldsymbol{\sigma}},\boldsymbol{\mu}^i,\boldsymbol{\gamma}^i), \tag{15}$$

$$\boldsymbol{\mu}^{i+1}=\arg\min_{\boldsymbol{\mu}}L_\delta(\hat{\boldsymbol{\sigma}},\boldsymbol{\mu}^i,\boldsymbol{\gamma}^i), \tag{16}$$

$$\boldsymbol{\gamma}^{i+1}=\boldsymbol{\gamma}^i+\hat{\boldsymbol{\sigma}}^{i+1}-\boldsymbol{\mu}^{i+1}, \tag{17}$$

where superscript i denotes the ith iteration.

After some mathematical derivations, the solutions for the sub-problems (15)−(17) are

$$\begin{cases}\hat{\boldsymbol{\sigma}}^{i+1}=(\boldsymbol{D}^{\mathrm{H}}\boldsymbol{D}+\delta\boldsymbol{I})^{-1}(\boldsymbol{D}^{\mathrm{H}}\boldsymbol{s}_{qn}+\delta(\boldsymbol{\mu}^i-\boldsymbol{\gamma}^i))\\ \boldsymbol{\mu}^{i+1}=S_{\lambda/\delta}(\hat{\boldsymbol{\sigma}}^{i+1}+\boldsymbol{\gamma}^i)\\ \boldsymbol{\gamma}^{i+1}=\boldsymbol{\gamma}^i+\hat{\boldsymbol{\sigma}}^{i+1}-\boldsymbol{\mu}^{i+1}\end{cases}. \tag{18}$$

Then, we can make the ADMM method to all the range bins and obtain the restored ISAR images.

3.2 Angular motion compensation

In the multi-static condition, there exist phase differences between different images. Hence we should make the image registration.

From Fig. 1, as the different locations of receivers A and B, the path length difference can be expressed as

$$(R_{TP}(t)+R_{PB}(t))-(R_{TP}(t)+R_{PA}(t))=$$
$$R_{PB}(t)-R_{PA}(t)=-L_r\sin\theta_{AB}(t). \tag{19}$$

Since the angle $\theta_{AB}(t)$ is small in this situation, (19) can be approximated to

$$(R_{TP}(t)+R_{PB}(t))-(R_{TP}(t)+R_{PA}(t))\approx-L_r\theta_{AB}(t) \tag{20}$$

Take Taylor expansion to the angle $\theta_{AB}(t)$:

$$\theta_{AB}(t)=\theta_{AB}(t_0)+\theta'_{AB}\cdot t \tag{21}$$

where θ'_{AB} denotes the first order term of Taylor series expansion.

Making FFT with regard to t_m in (8), we can obtain

$$s_B(\hat{f}, f_m)\mathrm{conj}\left(s_A(\hat{f}, f_m)\right) = \sum_{p=1}^{P}\sigma_{AB}\mathrm{sinc}\left(T_c\left(f_m - f_{pA} - \frac{f_c L_r \theta'_{AB}(t)}{\mathrm{c}}\right)\right)\cdot \exp\left(-\mathrm{j}\frac{2\pi f_c L_r \theta_{AB}(t_0)}{\mathrm{c}}\right) \tag{22}$$

where f_{pA} denotes the scatter p's frequency in receiver A, σ_{AB} denotes the amplitude, and T_c means the imaging time. To achieve the image co-registration, we need to compensate the term $f_c L_r \theta'_{AB}(t)/\mathrm{c}$ in (22) as

$$\tilde{s}_{Bd}(\hat{f}, t_m) = s_{Bd}(\hat{f}, t_m)\cdot\exp\left(-\mathrm{j}\frac{2\pi f_c L_r \theta'_{AB}(\mathrm{t})}{\mathrm{c}}\right). \tag{23}$$

From (23), we can see that the estimation of $\theta_{AB}(t)$ is a necessary step. In this paper, we employ the method in [22] to carry out the compensation process.

Furthermore, since L_r is usually much smaller than L_{tr}, the phase of estimated $\hat{\theta}_{AB}(t)$ has ambiguity and should be unwrapped as

$$\begin{cases} \hat{\hat{\theta}}_{AB}(1) = \hat{\theta}_{AB}(1) \\ \hat{\hat{\theta}}_{AB}(m+1) = \hat{\theta}_{AB}(m) + \Delta\hat{\theta}_{AB} \end{cases}, \tag{24}$$

$$\Delta\hat{\theta}_{AB}(\mathrm{t}) = \begin{cases} \hat{\theta}_{AB}(m+1) - \hat{\theta}_{AB}(m), & \left|\hat{\theta}_{AB}(m+1) - \hat{\theta}_{AB}(m)\right| < \pi \\ \hat{\theta}_{AB}(m+1) - \hat{\theta}_{AB}(m) + 2\pi, & \hat{\theta}_{AB}(m+1) - \hat{\theta}_{AB}(m) < -\pi \\ \hat{\theta}_{AB}(m+1) - \hat{\theta}_{AB}(m) - 2\pi, & \hat{\theta}_{AB}(m+1) - \hat{\theta}_{AB}(m) > \pi \end{cases}, \tag{25}$$

where $\hat{\hat{\theta}}_{AB}$ denotes the unwrapped phase.

The angular motion compensation is completed when the phase unwrapped processing is finished.

3.3 Flow of the proposed method

To achieve a satisfactory performance of 3D ISAR imaging for the observed ship under the sparse aperture situation, many processes need to be carried out. The concrete procedures are enumerated as follows:

Step 1 Acquire the original data from three receivers and making de-stretch process.

Step 2 Adopt the envelope alignment method based on minimum entropy and the phase correction method based on eigenvector to realize motion compensation under sparse aperture. Since the coherency between the three received signals is a key requirement to achieve 3D reconstruction, the aforementioned motion compensation methods need to be implemented for all three channel signals together.

Step 3 Perform ADMM to the sparse aperture data after motion compensation. By setting appropriate parameters, we can obtain the high resolution ISAR images.

Step 4 Carry out angular motion compensation and phase unwrapping process to the reconstructed signals to realize image co-registration. Then, matched images of targets can be obtained.

Step 5 Carry out the interferometric processing with respect to the images from three channels and obtain the 3D imaging results of the ship target with multi-static configuration under sparse aperture.

The details of this procedure are illustrated in Fig. 3.

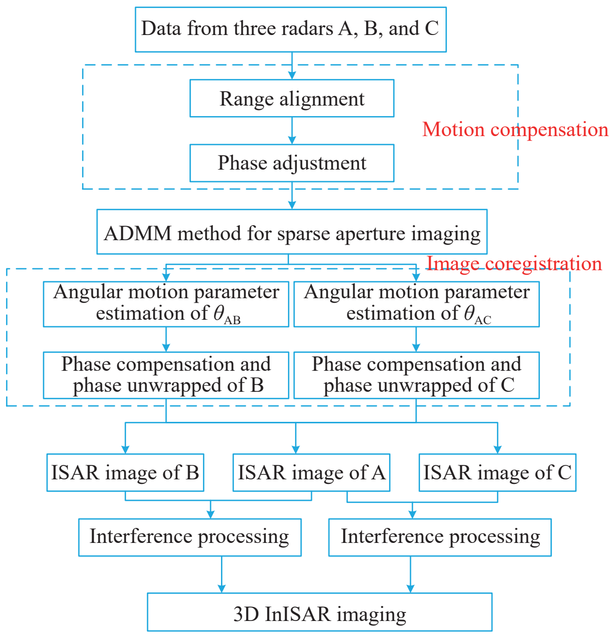

Fig. 3 Flowchart of multi-static 3D imaging method under sparse aperture

4. Experimental results

In this section, we conduct simulations to validate the proposed method. First, we utilize a sinusoidal signal to check out the performance of the ADMM algorithm under different SNRs and different sparsity rates (SRs). The parameters λ and δ are set as 0.1 and 1.0, respectively. The signal is formulated as

$$x = a\cdot\sin\left(2\pi f T_s t_s\right) \tag{26}$$

where a denotes the amplitude, f, T_s, t_s represent signal frequency, sampling interval, and sampling index, respectively.

Fig. 4 gives the ADMM method's root mean square error (RMSE) values versus different SNRs and SRs. When the estimated signal is close to the original signal, the RMSE will be small and vice versa.

From Fig. 4(a), we can see that the RMSE result decreases as the SNR increases. On the other side, Fig. 4(b) illustrates that the RMSE result increases when the sparsity rate goes up.

Then, we utilize a simulated ship target to explore the validity of the ship target. The ship target is modelled in Fig. 5. Fig. 5(a)–Fig. 5(c) are the ship’s three-view drawings. Fig. 5(d) illustrates the 3D model of the ship.

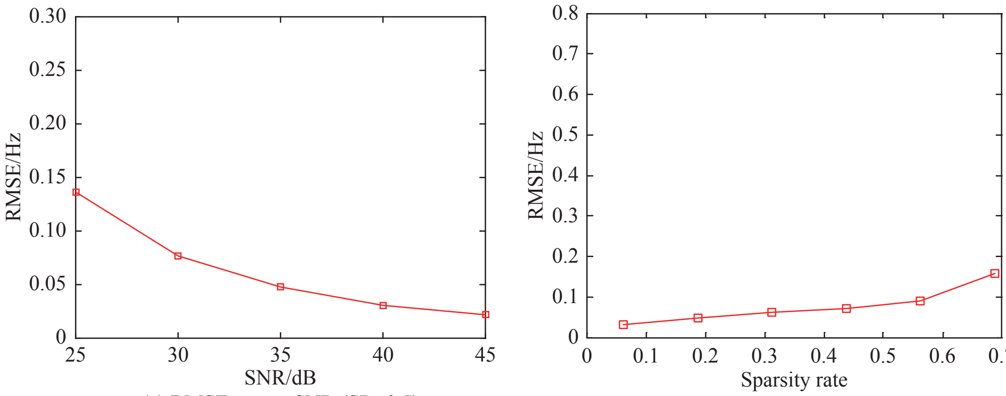

(a) RMSE versus SNR (SR=0.5)
(b) RMSE versus SR (SNR=30 dB)

Fig. 4 RMSEs of the ADMM method

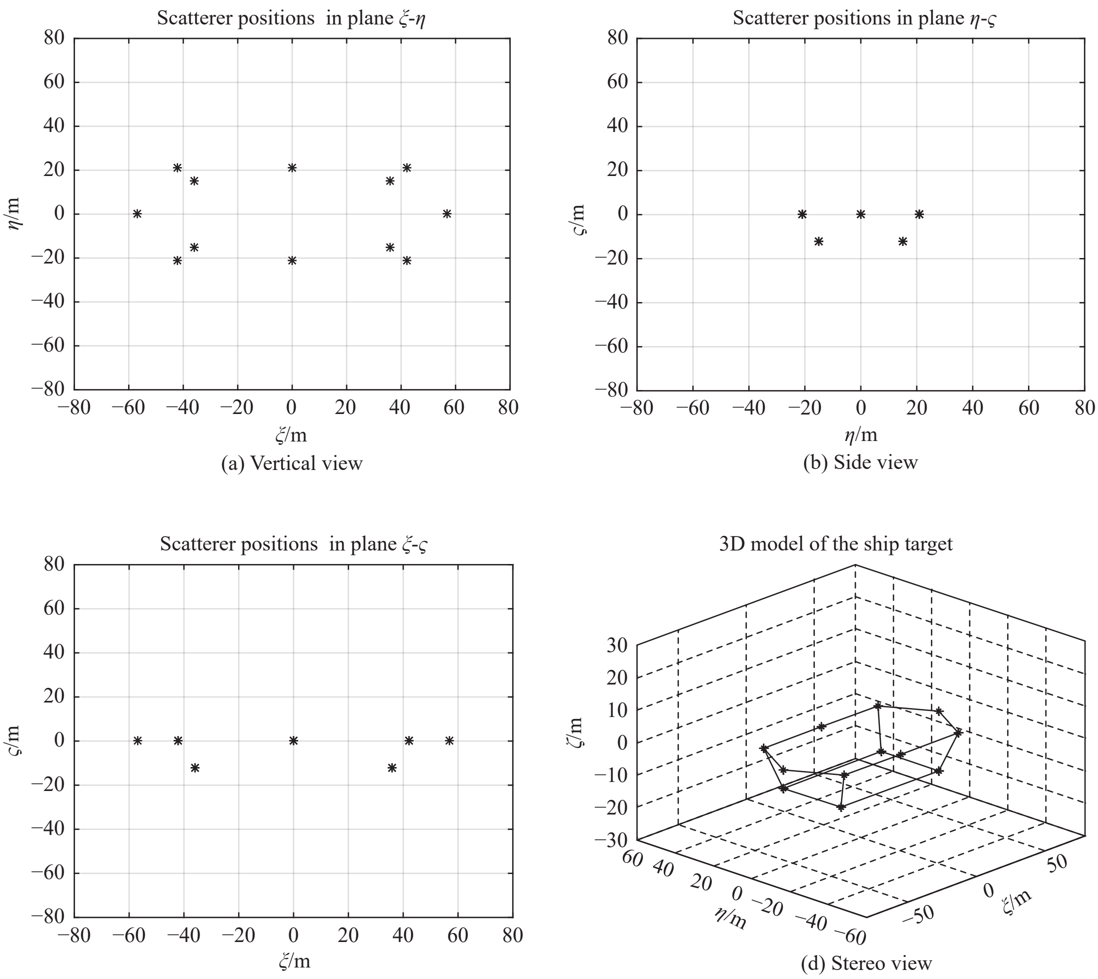

(a) Vertical view
(b) Side view
(c) Front view
(d) Stereo view

Fig. 5 Model of the ship

The parameters of radar system simulated in the paper are listed in Table 1. Referring to Fig. 1, the transmitter T, the receiver A, and the receiver B are situated in the U axis, while the receiver C is located in the W axis. The distance between transmitter T and the origin is 5 km. The initial target’s coordinates in the coordinate system

(O, U, V, W) are (U_0=0 m, V_0=10 km, W_0=0 m). The coordinate system (O, U, V, W) is parallel to the coordinate system (O', X, Y, Z). The ship's translational speed is 600 knots. The ship target is moving at an angle of 72° with regard to the U axis.

Table 1 Parameters of the radar system

Parameter	Value	Parameter	Value
Range sampling frequency/MHz	25.6	Bandwidth/MHz	200
SNR/dB	25	Carrier frequency/GHz	10
Pulse number	256	Pulse repetition frequency/Hz	625
Pulse width/μs	10	The length of baseline/m	2

Firstly, we explore the proposed method's effectiveness with one-rotational motion dominant. Table 2 illustrates the ship's three-dimensional rotation parameters with yaw motion being the dominant. Fig. 6 shows the ship's 3D multi-static InISAR images under the sparse aperture situation, with 128 echoes disappearing. It can be seen that the ADMM method is valid in signal reconstruction and its imaging performance under the sparse aperture condition with 50% missing data is satisfactory compared to the model and the imaging results with the whole data.

Table 2 3D rotation parameters of the ship with one dimension dominant

Parameter	Pitch	Roll	Yaw
Amplitude/radian	1π/180	1.5π/180	3π/180
Period/s	6	12	14
Angular velocity/(radian/s)	2π/6	2π/12	2π/14

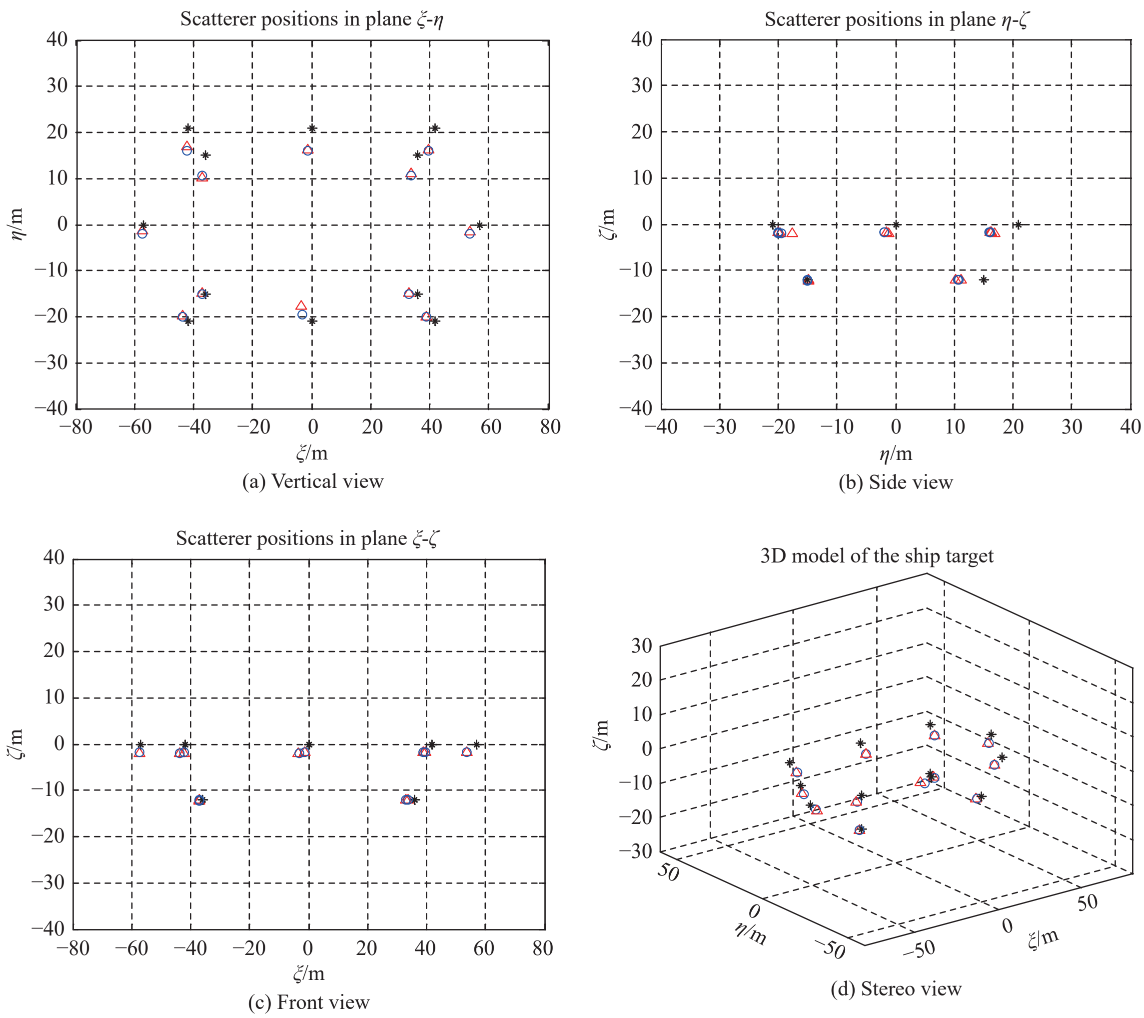

△ : Recovery; ∗ : Original; ○ : No missing.

Fig. 6 Three dimensional InISAR images of the ship under sparse aperture with one dimension dominant

Next, we demonstrate the validity of the proposed method with complex target motion. The relative ship's 3D rotational parameters are shown in Table 3, with large motion amplitudes in all pitch, roll, and yaw directions. The sparse situation is also 50% randomly missing data.

Table 3 3D rotation parameters of the ship with all dimensions dominant

Parameter	Pitch	Roll	Yaw
Amplitude/radian	2π/180	3π/180	4π/180
Period/s	6	12	14
Angular velocity/(radian/s)	2π/6	2π/12	2π/14

Fig. 7 shows the 3D multi-static InISAR ship target's images with complex target motion. The imaging results in Fig. 7 show that the recovered positions of points are similar to the original ones and the ones with no missing data, which demonstrates that the proposed method is still applicable when the target undergoes complex three-dimensional motion.

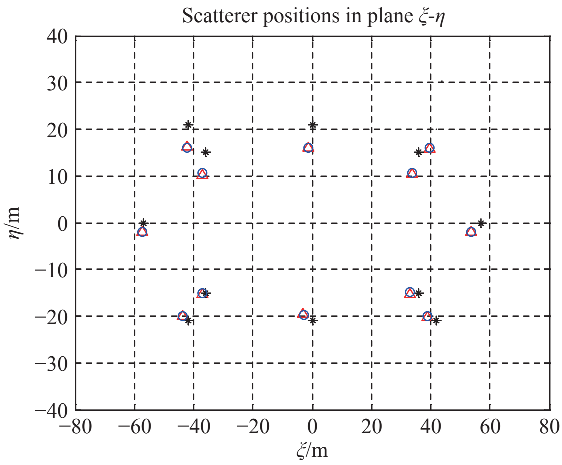

(a) Vertical view

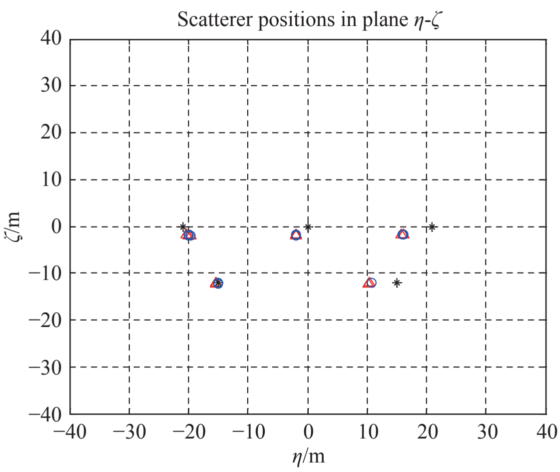

(b) Side view

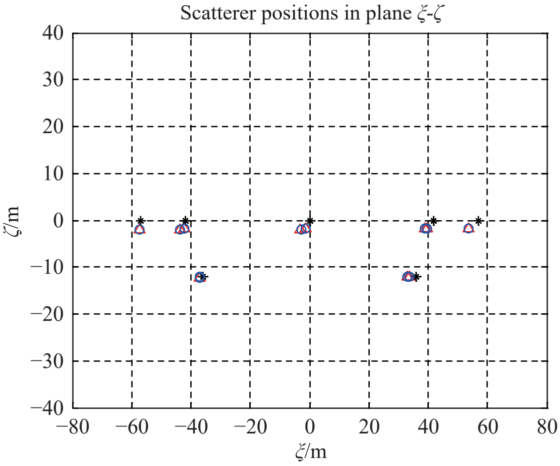

(c) Front view

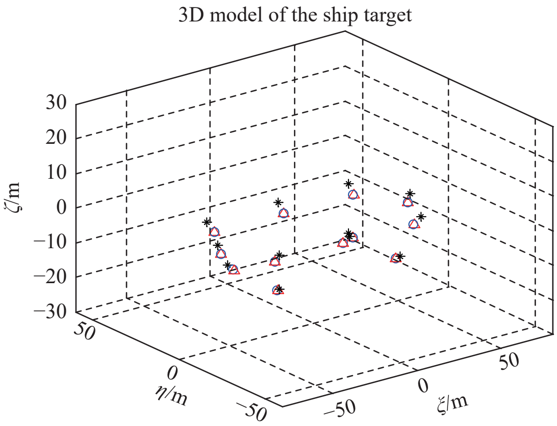

(d) Stereo view

△ : Recovery; ∗ : Original; ○ : No missing.

Fig. 7 Three dimensional InISAR images of the ship under sparse aperture with all dimensions dominant

Furthermore, in order to quantitatively access the proposed method's performance, we utilize the RMSE as the quantitative criterion.

The RMSE between the InISAR image obtained with the proposed method and the target model is defined as

$$\mathrm{RM} = \sqrt{\frac{1}{P}\sum_{p=1}^{P}\left[(\hat{x}_p - x_p)^2 + (\hat{y}_p - y_p)^2 + (\hat{z}_p - z_p)^2\right]} \quad (27)$$

where (x_p, y_p, z_p) denotes the scatterer p's coordinates in the target model. $(\hat{x}_p, \hat{y}_p, \hat{z}_p)$ denotes the coordinates of the scatterer p in the InISAR image acquired with the proposed method.

Similarly, the RMSE between the InISAR image obtained with the whole data and the target model is defined as

$$\mathrm{RM1} = \sqrt{\frac{1}{P}\sum_{p=1}^{P}\left[\left(\hat{\hat{x}}_p - x_p\right)^2 + \left(\hat{\hat{y}}_p - y_p\right)^2 + \left(\hat{\hat{z}}_p - z_p\right)^2\right]} \quad (28)$$

where $(\hat{\hat{x}}_p, \hat{\hat{y}}_p, \hat{\hat{z}}_p)$ denotes the coordinates of the scatterer

p in the InISAR image obtained with the whole data.

Table 4 gives the RM and RM1 results of Fig. 6 and Fig. 7.

Table 4 RMSE results of Fig. 6 and Fig. 7

Figure	RM	RM1
Fig. 6	3.8269	3.8036
Fig. 7	3.9546	3.8103

From Table 4, we can see that the RM results are close to the RM1 results in both situations, which further validate the effectiveness of the proposed method.

5. Conclusions

In this paper, we adopt the multi-static configuration to realize the ship targets' imaging under sparse aperture. The ADMM algorithm is utilized to restore the whole signal and produce the super resolution ISAR image. Furthermore, the InISAR technique is introduced to enhance the target recognition efficiency. Experimental results with the simulated data verify the validity of the proposed method.

References

[1] CHEN C C, ANDREWS H C. Target-motion induced radar imaging. IEEE Trans. on Aerospace and Electronic Systems, 1980, 16(1): 2–14.

[2] ZHENG J B, SU T, ZHU W T, et al. ISAR imaging of targets with complex motions based on the keystone time-chirp rate distribution. IEEE Geoscience and Remote Sensing Letters, 2014, 11(7): 1275–1279.

[3] LI G, ZHANG H, WANG X Q, et al. ISAR 2-D imaging of uniformly rotating targets via matching pursuit. IEEE Trans. on Aerospace and Electronic Systems, 2012, 48(2): 1838–1846.

[4] ZHENG J B, SU T, ZHANG L, et al. ISAR imaging of targets with complex motion based on the chirp rate-quadratic chirp rate distribution. IEEE Trans. on Geoscience and Remote Sensing, 2014, 52(11): 7276–7289.

[5] ZHENG J B, SU T, ZHU W T, et al. Fast parameter estimation algorithm for cubic phase signal based on quantifying effects of Doppler frequency shift. Progress in Electromagnetics Research, 2013, 142: 57–74.

[6] ZHANG L, DUAN J, QIAO Z J. Phase adjustment and ISAR imaging of maneuvering targets with sparse apertures. IEEE Trans. on Aerospace and Electronic System, 2014, 50(3): 1955–1973.

[7] ZENG C Z, ZHU W G, JIA X. Sparse aperture ISAR imaging algorithm based on adaptive filtering framework. IET Radar, Sonar & Navigation, 2019, 13(3): 445–455.

[8] PRICKETT M J, CHEN C C. Principles of inverse synthetic aperture radar imaging. Proc. of the Electronic Aerospace System Conference, 1980: 340–345.

[9] ZHU D Y, WANG L, YU Y, et al. Robust ISAR range alignment via minimizing the entropy of the average range profile. IEEE Geoscience and Remote Sensing Papers, 2009, 6(2): 204–208.

[10] WAHL D E, EICHEL P H, GHIGLIA D C, et al. Phase gradient autofocus—a robust tool for high-resolution SAR phase correction. IEEE Trans. on Aerospace and Electronic System, 1994, 30(3): 827–835.

[11] YE W, YEO T S, BAO Z. Weighted least-squares estimation of phase errors for SAR/ISAR autofocus. IEEE Trans. on. Geoscience and Remote Sensing, 1999, 37(5): 2487–2494.

[12] JAKOWATZ C V, WAHL D E. Eigenvector method for maximum-likelihood estimation of phase errors in synthetic aperture radar imagery. Journal of the Optical Society of America, 1993, 10(12): 2539–2546.

[13] MARTORELLA M, BERIZZI F, HAYWOOD B. Contrast maximization based technique for 2-D ISAR autofocusing. IEE Proceedings-Radar, Sonar and Navigation, 2005, 152(4): 253–262.

[14] LARSSON E G, STOICA P, LI J. Amplitude spectrum estimation for two-dimensional gapped data. IEEE Trans. on Signal Processing, 2002, 50(6): 1343–1353.

[15] BARANIUK R, STEEGHS P. Compressive radar imaging. Proc. of the IEEE Radar Conference, 2007: 128–133.

[16] DONOHO D L. Compressed sensing. IEEE Trans. on Information Theory, 2006, 52(4): 1289–1306.

[17] CANDES E J, ROMBERG J, TAO T. Robust uncertainty principles: exact signal reconstruction from highly incomplete frequency information. IEEE Trans. on Information Theory, 2006, 52(2): 489–509.

[18] MORADIKIA M, SAMADI S, CETIN M. Joint SAR imaging and multi-feature decomposition from 2-D under-sampled data via low-rankness plus sparsity priors. IEEE Trans. on Computational Imaging, 2018, 5(1): 1–16.

[19] QIU W, ZHOU J X, FU Q. Jointly using low-rank and sparsity priors for sparse inverse synthetic aperture radar imaging. IEEE Trans. on Image Processing, 2020, 29: 100–115.

[20] LU X Y, ZHAO Y J, YANG J C. An efficient method for single-channel SAR target reconstruction under severe deceptive jamming. IEEE Geoscience and Remote Sensing Letters, 2020, 17(2): 237–241.

[21] LI Y C, WU R, XING M D. Inverse synthetic aperture radar imaging of ship target with complex motion. IET Radar, Sonar & Navigation, 2008, 2(6): 395–403.

[22] WANG Y, LI X L. Three-dimensional interferometric ISAR imaging for the ship target under the bi-static configuration. IEEE Journal of Selected Topics in Applied Earth Observation and Remote Sensing, 2016, 9(4): 1505–1520.

[23] MA C Z, YEO T S, GUO Q. Bistatic ISAR imaging incorporating interferometric 3-D imaging technique. IEEE Trans. on Geoscience and Remote Sensing, 2012, 50(10): 3859–3867.

[24] QIU W, ZHOU J X, ZHAO H Z, et al. Three-dimensional sparse turntable microwave imaging based on compressive sensing. IEEE Geoscience and Remote Sensing Letters, 2015, 12(4): 826–830.

[25] XU G, XING M D, XIA X G. Three-dimensional geometry and motion estimations of maneuvering targets for interferometric ISAR with sparse aperture. IEEE Trans. on Image Processing, 2016, 25(5): 2005–2020.

[26] WU Y L, ZHANG S S, KANG H Q. Fast marginalized sparse Bayesian learning for 3-D interferometric ISAR image formation via super-resolution ISAR imaging. IEEE Journal of Selected Topics in Applied Earth Observations and Remote Sensing, 2015, 8(10): 4942–4951.

Biographies

JI Bingren was born in 1992. He received his B.S. degree and M.S. degree in the Department of Electronic Information Engineering in 2014 and 2016 from Harbin Institute of Technology (HIT), Harbin, China. He is now pursuing his Ph.D. degree in the Department of Electronic Information Engineering from HIT. His current research interests include ISAR imaging, compressed sensing, and interferometric ISAR.
E-mail: 1455252058@qq.com

WANG Yong was born in 1979. He received his B.S. degree and M.S. degree from Harbin Institute of Technology (HIT), Harbin, China, in 2002 and 2004, respectively, both in electronic engineering. He received his Ph.D. degree in information and communication engineering from HIT in 2008. He is currently a professor with the Institute of Electronic Engineering Technology in HIT. His main research interests are time frequency analysis of nonstationary signals, radar signal processing, and their application in synthetic aperture radar imaging.
E-mail: wangyong6012@hit.edu.cn

ZHAO Bin was born in 1972. He received his B. S. degree and M.S. degree from Harbin Institute of Technology (HIT), Harbin, China, in 1988 and 1998, respectively, both in electronic engineering. He received his Ph.D. degree in information and communication engineering from HIT in 2008. He is currently a professor with the Institute of Electronic Engineering Technology in HIT. His main research interests are radar system control and synthetic aperture radar imaging.
E-mail: smith@riee.hit.edu.cn

XU Rongqing was born in 1958. He received his B.S. and M.S. degrees in electronic engineering and his Ph.D. degree in information and communication engineering from Harbin Institute of Technology (HIT), Harbin, China, in 1982, 1984, and 1990, respectively. He is currently a professor with the Institute of Electronic Engineering Technology, HIT. His main research interest is radar signal processing.
E-mail: xurongqing@hit.edu.cn